HEPATOLOGY

HEPATOLOGY, VOL. 69, NO. 2, 2019

Neoplastic Transformation of the Peribiliary Stem Cell Niche in Cholangiocarcinoma Arisen in Primary Sclerosing Cholangitis

Guido Carpino ,[1*] Vincenzo Cardinale,[2*] Trine Folseraas,[3] Diletta Overi ,[4] Krzysztof Grzyb,[5] Daniele Costantini ,[6] Pasquale Bartolomeo Berloco,[7] Sabina Di Matteo,[6] Tom Hemming Karlsen,[3] Domenico Alvaro,[6**] and Eugenio Gaudio[4**]

Primary sclerosing cholangitis (PSC) is a chronic inflammatory cholangiopathy frequently complicated by cholangiocarcinoma (CCA). Massive proliferation of biliary tree stem/progenitor cells (BTSCs), expansion of peribiliary glands (PBGs), and dysplasia were observed in PSC. The aims of the present study were to evaluate the involvement of PBGs and BTSCs in CCA which emerged in PSC patients. Specimens from normal liver (n = 5), PSC (n = 20), and PSC-associated CCA (n = 20) were included. Samples were processed for histology, immunohistochemistry, and immunofluorescence. *In vitro* experiments were performed on human BTSCs, human mucinous primary CCA cell cultures, and human cholangiocyte cell lines (H69). Our results indicated that all CCAs emerging in PSC patients were mucin-producing tumors characterized by PBG involvement and a high expression of stem/progenitor cell markers. Ducts with neoplastic lesions showed higher inflammation, wall thickness, and PBG activation compared to nonneoplastic PSC-affected ducts. CCA showed higher microvascular density and higher expression of nuclear factor kappa B, interleukin-6, interleukin-8, transforming growth factor β, and vascular endothelial growth factor-1 compared to nonneoplastic ducts. CCA cells were characterized by a higher expression of epithelial-to-mesenchymal transition (EMT) traits and by the absence of primary cilia compared to bile ducts and PBG cells in controls and patients with PSC. Our *in vitro* study demonstrated that lipopolysaccharide and oxysterols (PSC-related stressors) induced the expression of EMT traits, the nuclear factor kappa B pathway, autophagy, and the loss of primary cilia in human BTSCs. *Conclusion:* CCA arising in patients with PSC is characterized by extensive PBG involvement and by activation of the BTSC niche in these patients, the presence of duct lesions at different stages suggests a progressive tumorigenesis. (Hepatology 2019;69:622-638).

Cholangiocarcinoma (CCA) represents the second most frequent type of primary liver cancer and comprises malignancies with high intertumor and intratumor heterogeneities.[1] CCA is currently classified into intrahepatic, perihilar, and distal types, based on the anatomical location.[1] Typical features of CCA are high expression of cancer stem cell markers and epithelial-to-mesenchymal

Abbreviations: BTSC, biliary tree stem/progenitor cell; CCA, cholangiocarcinoma; DYS, dysplasia; EMT, epithelial-to-mesenchymal transition; EpCAM, epithelial cell adhesion molecule; Gli-1, glioma-associated oncogene 1; h-, human; γH2A.x, gamma H2A histone family, member x; HDAC6, histone deacetylase 6; IBD, inflammatory bowel disease; IF, immunofluorescence; IHC, immunohistochemistry; IκB, inhibitor of kappa B; IL, interleukin; K, keratin; KM, Kubota's medium; LC3, light chain 3; LPS, lipopolysaccharide; MVD, microvascular density; MTS, 3-(4,5-dimethylthiazol-2-yl)-5-(3-carboxymethoxyphenyl)-2-(4-sulfophenyl)-2H-tetrazolium; NF-κB, nuclear factor kappa B; OCT4A, octamer-binding transcription factor 4A; p-, phosphorylated; PAS, periodic acid–Schiff; PBG, peribiliary gland; PCNA, proliferating cell nuclear antigen; PSC, primary sclerosing cholangitis; SALL4, Sal-like protein 4; αSMA, alpha smooth muscle actin; SOX, Sry-related HMG box; TGF-β, transforming growth factor beta; VEGF, vascular endothelial growth factor; vWF, von Willebrand factor; WB, western blot.

Received April 18, 2018; accepted July 26, 2018.

Additional Supporting Information may be found at onlinelibrary.wiley.com/doi/10.1002/hep.30210/suppinfo.

**These authors contributed equally to this work as co-first authors.*

***These authors contributed equally to this work as co-senior authors.*

Supported by a research project grant from Sapienza University of Rome (to E.G.) and by Consorzio Interuniversitario Trapianti d'Organo (Rome, Italy), a sponsored research agreement from Vesta Therapeutics (Bethesda, MD), and the Norwegian PSC Research Center (Oslo, Norway).

transition (EMT) traits.[2] Moreover, CCA is characterized by a prominent desmoplastic stroma composed of cancer-associated fibroblasts, inflammatory cells, and vascular cells.[3,4] CCA development is strongly associated with chronic inflammatory conditions of the large bile ducts,[5] such as primary sclerosing cholangitis (PSC) and biliary liver fluke infestation.[5,6]

PSC is a cholangiopathy characterized by chronic inflammation which primarily affects extrahepatic and large intrahepatic bile ducts, leading to concentric periductal fibrosis and obliterating strictures.[7-9] In developed countries, PSC is the most common risk factor for CCA, and patients with PSC carry a 400-fold higher risk for CCA development compared to the general population.[7] Among patients with PSC, the annual risk of CCA is nearly 2% and the 30-year cumulative incidence is 20%.[7]

Recently, the involvement of biliary tree stem/progenitor cells (BTSCs) has been demonstrated in the progression of typical PSC duct lesions.[9] BTSCs represent a stem/progenitor cell niche located within the glands of the biliary tree (peribiliary glands [PBGs]).[7,10-12] A massive BTSC proliferation was revealed in PSC, and the subsequent PBG hyperplasia contributes to bile duct wall thickening, leading to obliterative fibrosis and strictures.[9,12] In PSC, PBGs showed signs of dysplasia and have been suggested as a possible cell of origin for CCA and biliary intraductal papillary mucinous neoplasms.[12]

Therefore, this study aimed to evaluate the involvement of PBGs and associated BTSCs in CCA emerging in patients with PSC and, in particular, to 1) characterize PSC-associated CCA (PSC-CCA) in terms of histological subtypes, PBG involvement, and stem cell marker expression; 2) evaluate the presence of multifocal preneoplastic lesions in surrounding tissues; 3) study possible associations between CCA emergence and features of chronic damage in bile ducts and peribiliary vascular plexus; and 4) investigate, *in vitro* and *in vivo*, the expression of EMT traits, the loss of primary cilia, and autophagy in BTSCs and tumor cells.

Materials and Methods

HUMAN SAMPLES

Formalin-fixed and paraffin-embedded liver tissues from patients with PSC were obtained from the Norwegian PSC Research Center, Division of Cancer, Surgery and Transplantation, Oslo University Hospital Rikshospitalet, Oslo, Norway, and from the "Paride

View this article online at wileyonlinelibrary.com.
DOI 10.1002/hep.30210

Potential conflict of interest: Nothing to report.

ARTICLE INFORMATION:

From the [1]Department of Movement, Human and Health Sciences, Division of Health Sciences, University of Rome "Foro Italico", Rome, Italy; [2]Department of Medico-Surgical Sciences and Biotechnologies, Sapienza University of Rome, Latina, Italy; [3]Norwegian PSC Research Center, Department of Transplantation Medicine, Division of Surgery, Inflammatory Medicine and Transplantation, Institute of Clinical Medicine, Faculty of Medicine, University of Oslo, Research Institute of Internal Medicine, Division of Surgery, Inflammatory Medicine and Transplantation, Oslo University Hospital Rikshospitalet, K.G. Jebsen Inflammation Research Centre, Institute of Clinical Medicine, Faculty of Medicine, University of Oslo, Oslo, Norway; [4]Department of Anatomical, Histological, Forensic Medicine and Orthopedic Sciences, Sapienza University of Rome, Rome, Italy; [5]Department of Pathology, Oslo University Hospital, Oslo, Norway; [6]Department of Medicine and Medical Specialties; [7]Department of General Surgery and Organ Transplantation, Sapsienza University of Rome, Rome, Italy.

ADDRESS CORRESPONDENCE AND REPRINT REQUESTS TO:

Guido Carpino, M.D., Ph.D.
Department of Movement, Human and Health Sciences
Division of Health Sciences
University of Rome "Foro Italico", Piazza Lauro De Bosis 6
00135 Rome, Italy
Tel.: +39-06-36733202
E-mail: guido.carpino@uniroma1.it

Stefanini" Department of General Surgery and Organ Transplantation, Sapienza University of Rome, Rome, Italy. Livers with normal histology were obtained from organ donors from the "Paride Stefanini" Department of General Surgery and Organ Transplantation, Sapienza University of Rome, Rome, Italy.

Specimens included (1) livers with normal histology from liver donors (n = 5), (2) explant livers obtained from patients with PSC (n = 20), (3) explant livers obtained from patients with PSC-CCA (n = 20). For liver specimens, the presence of at least 10 complete portal tracts was required. For large bile ducts, the complete transversal section of the wall was needed; tumor samples were considered adequate when at least five nonoverlapping microscopic fields at ×20 magnification could be examined in the same section. Written informed consent was obtained from each patient, and the study protocol conformed to the ethics guidelines of the 1975 Declaration of Helsinki. The research protocol was reviewed and approved by the ethics committees of Umberto I Policlinico of Rome, Italy, and the regional committees for medical and health research ethics in southeastern Norway. No donor organs were obtained from executed prisoners or other institutionalized persons. Patients and tumor characteristics are indicated in Supporting Table S1.

LIGHT MICROSCOPY, HISTOPATHOLOGY, AND IMMUNOHISTOCHEMISTRY

Tissue sections were stained with hematoxylin and eosin, periodic acid–Schiff (PAS), and sirius red, according to standard protocols. Immunohistochemistry (IHC) and immunofluorescence (IF) were performed as described,[9,13] and complete methodology is provided in Supporting Information. A list of primary antibodies is reported in Supporting Table S2. All slides were scanned by a digital scanner (Aperio Scanscope CS System, Aperio Digital Pathology; Leica Biosystems, Milan, Italy) and processed by ImageScope software.

The area occupied by keratin (K) 7$^+$ PBGs was quantified by an image analysis algorithm and expressed as the percentage of the total area.[9,13] Expression of nuclear antigens and membrane expression of epithelial cell adhesion molecule (EpCAM) were automatically calculated by specific algorithms on the entire section and expressed as percentage of positive cells. Microvascular density (MVD) was calculated as the area occupied by von Willebrand factor (vWF)$^+$ vessels quantified by an image analysis algorithm and expressed as extension (square micrometers per square millimeter of tissue).

For the other immunoreactions, the percentage of positive cells was automatically calculated by an algorithm on the entire section; furthermore, a semiquantitative scoring system was applied (0, <5%; 1, 5%-10%; 2, 11%-30%; 3, 31%-50%; 4, >50%).[9] In some figures, the semiquantitative score was used to visualize data obtained from IHC stains and is reported in a color gradient heat map where each gradient represents statistically significant differences among groups.[14] Percentage and scores of positive cells are included in Table 1.

HUMAN CELLS

Human (h) BTSCs were isolated from extrahepatic biliary tree as described.[15,16] CCA cells were isolated from large bile duct–type (mucinous) CCA samples as described.[2,17] H69 cells, an SV40-transformed (i.e., immortalized) human cholangiocyte cell line, were grown in H69 medium and used as a positive control for the presence of primary cilia.[18]

hBTSCs were cultured in Kubota's medium (KM), a serum-free medium developed for survival and expansion of endodermal stem/progenitors.[2,15] Then, hBTSCs were conditioned by adding selected PSC-associated endogenous and exogenous stressors to KM for 10 days. The factors were lipopolysaccharide (LPS; 200 ng/mL) or oxysterols (proinflammatory/oxidative bile compounds; cholest-4,6-dien-3-one, 0.14 mM). Concentrations of tested compounds were chosen based on previous literature[19-22]; cells were exposed for a prolonged period (10 days) to mimic chronic stimulation occurring in PSC. Enriched conditioned medium was changed every 2 days. After 10 days, cells were detached for analyses. In further experiments, the autophagy inhibitor wortmannin (W1628; Sigma-Aldrich; 100 nM) was added to the above-mentioned media for 4 hours.[23] Media, solutions, and complete methods for cell viability, colony counting, population doubling time, 3-(4,5-dimethylthiazol-2-yl)-5-(3-carboxymethoxyphenyl)-2-(4-sulfophenyl)-2*H*-tetrazolium (MTS) assay, RT-PCR, and western blot (WB) are detailed in the Supporting Information.

TABLE 1. Percentage and Semiquantitative Score of Positive Cells Within Peribiliary Glands for Given Antigens

	Normal	PSC	PSC-CCA
mEpCAM	43.7 ± 6.1%	74.7 ± 4.04%*	19.3 ± 4.16%*
(score)	(3)	(4)	(2)
SOX9	16.0 ± 4.2%*	39.4 ± 4.4%	42.0 ± 8.4%
(score)	(2)	(3)	(3)
SALL4	1.8 ± 1.6%	8.6 ± 1.9%*	19.0 ± 8.2%*
(score)	(0)	(1)	(2)
OCT4A	3.6 ± 1.3%	4.6 ± 2.32%	15.75 ± 4.4%*
(score)	(0)	(0)	(2)
VEGF	1.2 ± 0.4%*	27.8 ± 12.8%	22.6 ± 11.2%
(score)	(0)	(2)	(2)
IL-8	1.0 ± 1.4%	19 ±4.2%*	43.0 ± 7.6%*
(score)	(0)	(2)	(3)
pNF-κB	21.1 ± 6.6%*	51.6 ± 13.3%	59.2 ± 10.1%
(score)	(2)	(4)	(4)
pIκB-α	1.6 ± 1.1%*	37.0 ± 6.1%	36.8 ± 3.8%
(score)	(0)	(3)	(3)
IL-6	6.0 ± 2.7%	30.0 ± 14.7%*	56.3 ± 4.8%*
(score)	(1)	(3)	(4)
TGF-β	1.2 ± 0.4%*	17.8 ± 5.3%	22.0 ± 7.7%
(score)	(0)	(2)	(2)
αSMA	0.4 ± 0.6%	9.2 ± 2.4%*	25.0 ± 7.3%*
(score)	(0)	(1)	(2)
N-Cadherin	0.2 ± 0.5%	6.2 ± 2.9%*	15.6 ± 4.2%*
(score)	(0)	(1)	(2)
Primary cilium	45.2 ± 8.7%	44.0 ± 9.4%	0.4 ± 0.5%*
(score)	(3)	(3)	(0)
Gli-1	6.4 ± 2.9%*	71.6 ± 5.9%	67.4 ± 9.9%
(score)	(1)	(4)	(4)
HDAC6	5.8 ± 2.6%	7.8 ± 1.9%	36.7 ± 7.1%*
(score)	(1)	(1)	(3)
LC3	3.2 ± 1.3%	12.5 ± 5.0%*	40.0 ± 7.1%*
(score)	(0)	(2)	(3)
p62	2.8 ± 1.9%	22.8 ± 5.7%*	42.6 ± 6%*
(score)	(0)	(2)	(3)
γH2A.X	3.0 ± 1.6%*	23.2 ± 6.6%	24.2 ± 5.8%
(score)	(0)	(2)	(2)

Data are expressed as percentage (mean ± standard deviation) and relative semiquantitative score in parentheses. The semiquantitative scoring system was as follows: 0, <5%; 1, 5%-10%; 2, 11%-30%; 3, 31%-50%; 4, >50%.
*$p < 0.05$ versus other groups.
Abbreviation: m-, membranous.

STATISTICAL ANALYSIS

Data are indicated as mean ± standard deviation. The Student *t* test or Mann-Whitney U test was used to determine differences between groups for normally or not normally distributed data, respectively. The Pearson correlation coefficient or the Spearman nonparametric correlation was used. $P < 0.05$ was considered statistically significant. Analyses were performed using SPSS software (IBM, Armonk, USA).

Results

HISTOMORPHOLOGICAL FEATURES OF CCAs AND PBG INVOLVEMENT

The histomorphological aspects of CCAs emerging in PSC patients were evaluated by hematoxylin and eosin, PAS, and K7/19 stains (Fig. 1). In all tumors, cells formed large gland-like structures located within the lamina propria of extrahepatic and large intrahepatic bile ducts. Tumor glandular elements were composed of tall (cuboidal to cylindrical) cells characterized by mucin production (PAS positivity) and K7/19 positivity. Tumor glands completely substituted PBGs residing in the lamina propria (periductal infiltrating growth) of bile ducts at the hilum (perihilar CCA) and of large intrahepatic bile ducts (i.e., segmental ducts, intrahepatic CCA) both in the presence and in the absence of tumor cells within surface epithelium (Supporting Fig. S1). In some cases, normal PBGs could be found in between tumor elements (Fig. 1A). In 4/20 cases, tumor gland-like elements were revealed in smaller portal spaces within surrounding liver parenchyma as a sign of longitudinal growth/spreading along the intrahepatic biliary tree (Supporting Fig. S2A); 3/20 tumors showed limiting plate infiltration and liver parenchyma invasion (Supporting Fig. S2B), a histological aspect that parallels the mass-forming growth pattern at gross examination. PAS positivity and cytokeratin profile were maintained by tumor cells invading the limiting plate, spreading along the intrahepatic biliary tree, or invading neighboring organs (Supporting Fig. S2C,D). In sum, based on histopathological features, all examined CCAs in patients with PSC could be classified as large bile duct–type (mucinous) CCAs; they invariably involved PBGs and showed longitudinal growth (i.e., periductal infiltration) along the biliary tree and/or infiltration of the surrounding liver parenchyma (i.e., mass-forming growth).

In all patients, the study of the surrounding liver parenchyma and biliary tree revealed that the large

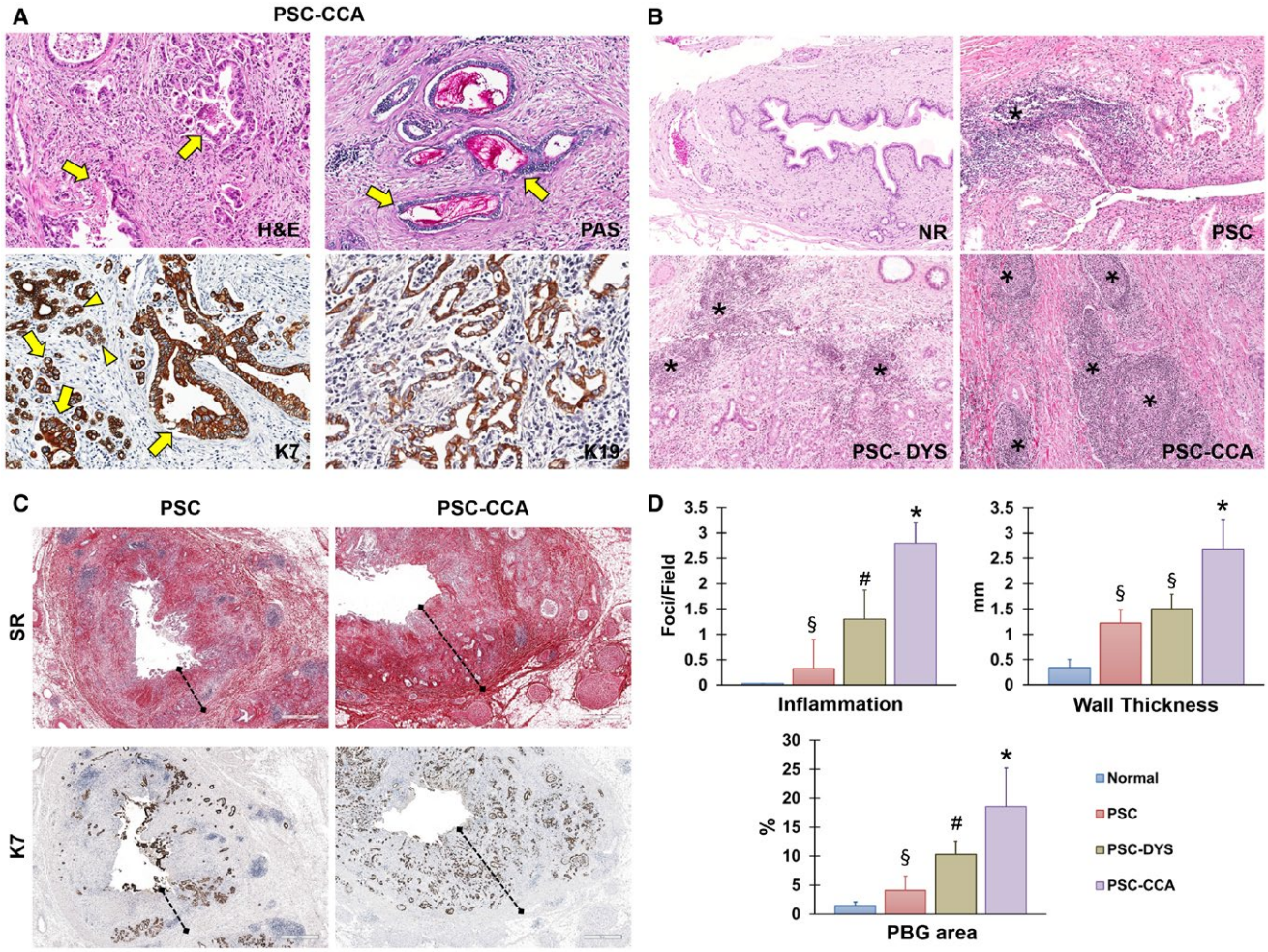

FIG. 1. Phenotype of PSC-CCA. (A) Hematoxylin and eosin, PAS, and IHC for biliary K7/K19 in PSC-CCA. In all tumors (PSC-CCA), cells formed large gland-like structures located within the lamina propria of hepatic and larger intrahepatic bile ducts (arrows). Tumor gland-like elements were composed of tall (cuboidal to cylindrical) cells characterized by mucinous production (PAS positivity, arrows). IHC for K7 and K19 shows that tumor glands completely substituted PBGs in the lamina propria of bile duct (arrows). Normal PBGs can be occasionally found in between tumor elements (arrowhead). Original magnification, ×20. (B) Hematoxylin and eosin in specimens obtained from normal subjects and from patients affected by PSC. In PSC patients, large intrahepatic and hepatic ducts with dysplastic (PSC-DYS) or neoplastic (PSC-CCA) lesions were studied and compared. Inflammation (asterisks) was higher in ducts with CCA compared to ducts without CCA and to ducts with dysplasia. Original magnification, ×10. (C) Sirius red and IHC for K7 in PSC patients and in CCA arisen in PSC patients (serial sections). The thickness of bile duct walls (dotted line) was increased in PSC-CCA samples compared to PSC specimens due to the marked expansion of $K7^{+}$ neoplastic PBG acini within duct walls (brownish structures). Original magnification, ×2. (D) Histograms show differences among examined ducts. Inflammation, wall thickness, and PBG area progressively increased in PSC ducts, with maximum values in ducts affected by CCA. $^{*}P < 0.05$ compared to other groups, $^{\#}P < 0.05$ compared to PSC and normal groups, $^{\S}P < 0.05$ compared to normal group. Abbreviations: H&E, hematoxylin and eosin; NR, normal; SR, sirius red.

intrahepatic (segmental and area) bile ducts were characterized by typical PSC lesions. Moreover, tissue specimens categorized as nonneoplastic at gross examination (so-called surrounding tissue) obtained from PSC patients with CCA showed a complete spectrum of lesions in the same patient, ranging from ducts with no or minimal inflammation to ducts with progressive inflammation and fibrosis to ducts with dysplasia and to neoplastic lesions. Remarkably, the presence of synchronous tumor and preneoplastic lesions (i.e., dysplasia in PBGs, biliary intraductal neoplasia, or papillary intraductal lesions) was observed in large intrahepatic ducts within surrounding tissue of all patients (Supporting Fig. S3).

HISTOPATHOLOGICAL FEATURES IN PSC AND PSC-CCA

Normal large intrahepatic and hilar bile ducts and ducts affected by PSC, by PSC-associated dysplastic lesions (PSC-DYS), and by PSC-CCA were studied and compared (Fig. 1; Supporting Figs. S4 and and Table S4). The number of inflammatory infiltrates was increased in PSC-CCA compared to ducts without CCA (Fig. 1B,D; see also Supporting Fig. S4). Moreover, the thickness of bile duct walls was increased in PSC compared to normal specimens (Fig. 1; Supporting Table S4). Ducts affected by PSC-CCA had thicker walls when compared to ducts affected by PSC and by PSC-DYS. The thickening in PSC-CCA samples was associated with the increased extension of neoplastic PBG acini in the stroma (Fig. 1C,D; see also Supporting Fig. S5). In keeping with this, PBG mass was progressively increased in PSC-CCA (14.4 ± 6.4%) compared to PSC-DYS (8.7 ± 2.5%, $P < 0.05$) and to PSC ducts (5.4 ± 1.5%, $P < 0.05$). In PSC ducts, PBG mass showed a positive correlation with the entity of inflammatory infiltrate ($r = 0.774$, $P < 0.01$). Similarly, the proliferation index of PBG cells, calculated by IHC for proliferating cell nuclear antigen (PCNA), was progressively higher in neoplastic PBGs compared to dysplastic PBGs and to PBGs in PSC ducts (Fig. 2A,C; Supporting Table S4).

EXPRESSION OF STEM CELL MARKERS IN PSC AND PSC-CCA

PSC-CCAs were investigated for typical markers of hepatic mature cells (K7, K19 for biliary lineage, and hepatocyte paraffin-1 for hepatocytic lineage) and putative stem cell markers. All CCAs in patients with PSC were composed of cells that were almost all positive for biliary keratins (Fig. 1) but virtually negative for the hepatocyte marker hepatocyte paraffin-1 (Supporting Fig. S6).

In regard to stem cell markers, CCA tumor elements were characterized by the modification of EpCAM expression (Fig. 2B,C and Table 1; Supporting Fig. S7). In particular, PSC-CCA showed a lower percentage of cells with a membranous expression pattern (19.3 ± 4.16%) compared to proliferating PBGs in PSC-affected ducts (74.7 ± 4.04%, $P < 0.05$); the EpCAM positivity was lower in CCA glandular elements invading deeply the lamina propria (20 ± 9.4%) in comparison with tumor elements located near the surface epithelium (40.5 ± 9.2%, $P < 0.05$). Moreover, expression of Sry-related HMG box (SOX) 9 was increased in PSC (39.4 ± 4.4%) and PSC-CCA (42.0 ± 8.4%) compared to normal ducts (16 ± 4.2%, $P < 0.05$; Fig. 2D,F and Table 1; Supporting Fig. S8). Tumors were almost negative for neural cell adhesion molecule (Supporting Fig. S6).

CCAs were highly positive for Sal-like protein 4 (SALL4; Fig. 2E,F), with >50% of neoplastic cells being positive; particularly, the nuclear expression of SALL4 was higher in PSC-CCA (19 ± 8.2%) compared to normal samples (1.8.0 ± 1.6%, $P < 0.01$; Supporting Fig. S8) and PSC samples (8.6 ± 1.9%, $P < 0.01$). PSC-CCAs also diffusely expressed pluripotency markers. Octamer-binding transcription factor 4A (OCT4A; Fig. D,F and Table 1) was expressed at the nuclear level in a subpopulation of CCA cells (15.75 ± 4.4%); this percentage was higher compared to PBGs in PSC-affected ducts (4.6 ± 2.32%, $P < 0.05$) and normal ducts (3.6 ± 1.3%, $P < 0.05$; Supporting Fig. S8). In addition, OCT4A was significantly more expressed in tumor cells invading the limiting plate and in cells infiltrating smaller portal spaces (43.4 ± 8.1%, $P < 0.05$; Supporting Fig. S9). Moreover, Tra-1-60 was diffusely and strongly expressed in tumor cells with both a cytoplasmic and an apical pattern (Supporting Fig. S6).

MICROVASCULAR EXPANSION AND INFLAMMATORY PATHWAYS IN PSC AND PSC-CCA

MVD was higher in PSC-affected ducts (7,663 ± 4,663 $\mu m^2/mm^2$) and in PSC-CCA samples (7,395 ± 5,108 $\mu m^2/mm^2$) compared to normal ducts (2,299 ± 880 $\mu m^2/mm^2$, $P < 0.05$; Fig. 3A). In addition, MVD correlated with inflammatory infiltrate in PSC ($r = 0.580$, $P < 0.05$) and in PSC-CCA ($r = 0.47$, $P < 0.05$) and with neoplastic PBG area in PSC-CCA samples ($r = 0.85$, $P < 0.01$). Consistently, vascular endothelial growth factor (VEGF) expression by PBGs (Fig. 3B,E and Table 1) was higher in PSC and PSC-CCA (27.8 ± 12.8% and 22.6 ± 11.2%, respectively) compared to normal samples (1.2 ± 0.4%, $P < 0.05$; Supporting Fig. S8). In patients with CCA, VEGF expression by tumor glandular elements was correlated with MVD ($r = 0.87$, $P < 0.01$), PBG mass ($r = 0.885$, $P < 0.05$), PBG proliferation index ($r = 0.62$,

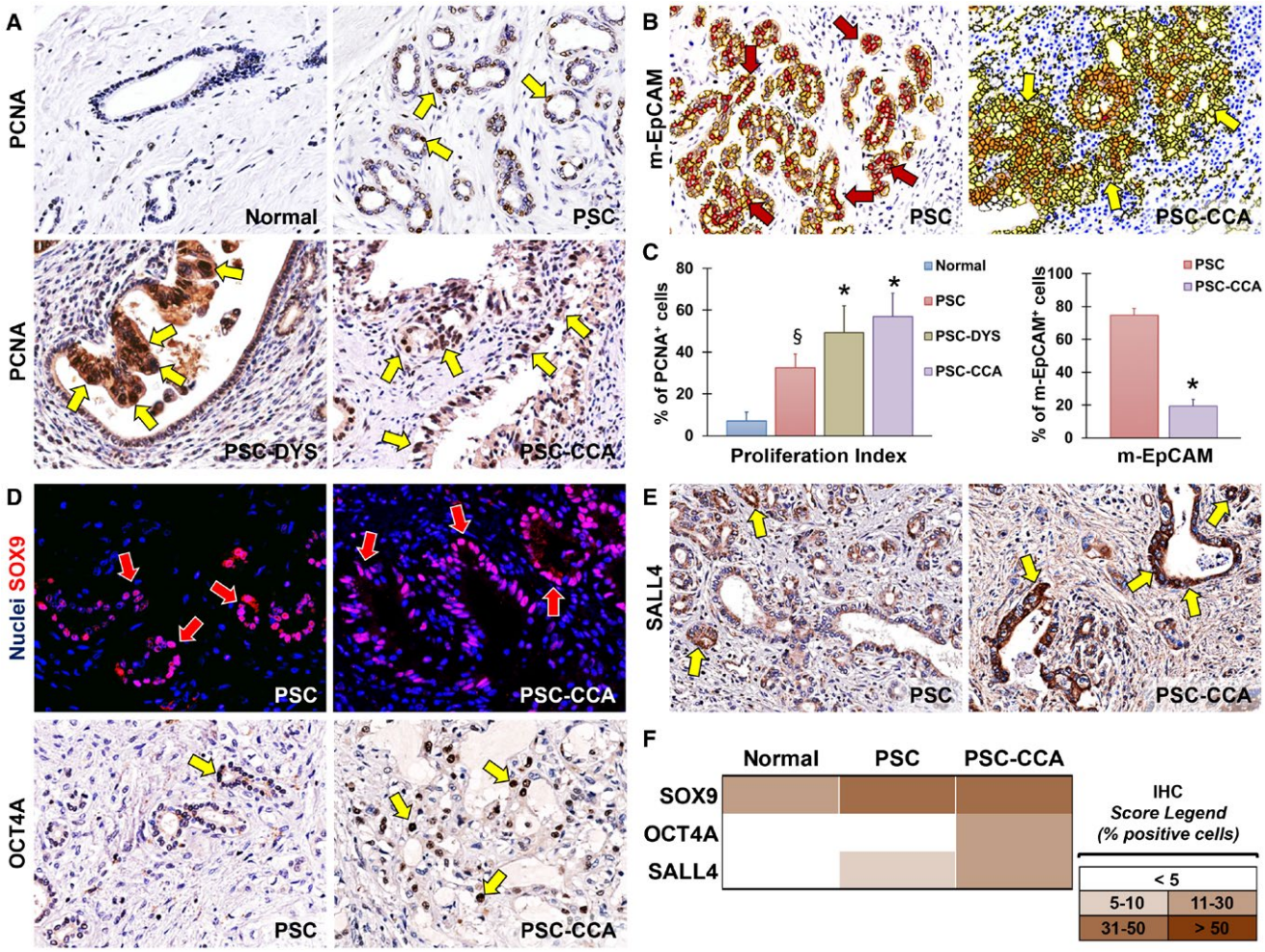

FIG. 2. Proliferation and stem cell markers in PSC-CCA. (A) IHC for PCNA in normal ducts, in ducts affected by PSC, in PSC-DYS ducts, and in PSC-CCA ducts affecting PBGs. PCNA expression (arrows) was low in normal ducts, while it was higher in neoplastic PBGs compared to dysplastic PBGs and to PBGs in ducts only affected by PSC. Original magnification, ×20. (B) IHC for EpCAM in ducts affected by PSC and in ducts with CCA. The membranous pattern expression was quantified by an image analysis algorithm. Red color (red arrows) generated by the algorithm indicates high membranous positivity, while orange and yellow indicate moderate to low membrane positivity (yellow arrows), respectively. In CCA, tumor glands showed a modified expression pattern characterized by a lower percentage of cells with membranous positivity compared to proliferating PBGs in PSC ducts without CCA lesions. Clean images without algorithm outputs are present in the Supporting Information. Original magnification, ×10. (C) Histograms show differences in PCNA and membranous EpCAM expression among examined groups. $^{*}P < 0.05$ compared to PSC and normal groups, $^{\S}P < 0.05$ compared to normal group. (D) IF for SOX9 (upper images) and IHC for OCT4A (lower images). CCAs were extremely rich in cells expressing stem cell markers (arrows). Original magnification, ×40. In IF (SOX9), nuclei are displayed in blue. (E) IHC for SALL4. CCAs were extremely rich in cells expressing SALL4 with a cytoplasmic and nuclear (arrows) pattern. Original magnification, ×40. (F) Heat map for visual representation of IHC/IF results obtained for given markers. IHC scores are reported as a color gradient heat map, where different colors represent statistically significant differences among groups. Representative images from controls are included in the Supporting Information. Abbreviation: m-, membranous.

$P < 0.05$), and inflammation ($r = 0.69$, $P < 0.05$). Moreover, expression of interleukin 8 (IL-8; Fig. 3B and Table 1), involved in both inflammation and angiogenesis, was higher in tumor glands (43.0 ± 7.6%) and in PBGs in PSC-affected ducts (19.0 ± 4.2%) compared to normal samples (1.0 ± 1.4%, $P < 0.01$; Supporting Fig. S8); PSC-CCA showed higher IL-8 expression compared to PBGs in PSC samples ($P < 0.05$).

We further evaluated the expression of phosphorylated nuclear factor kappa B (pNF-κB), phosphorylated

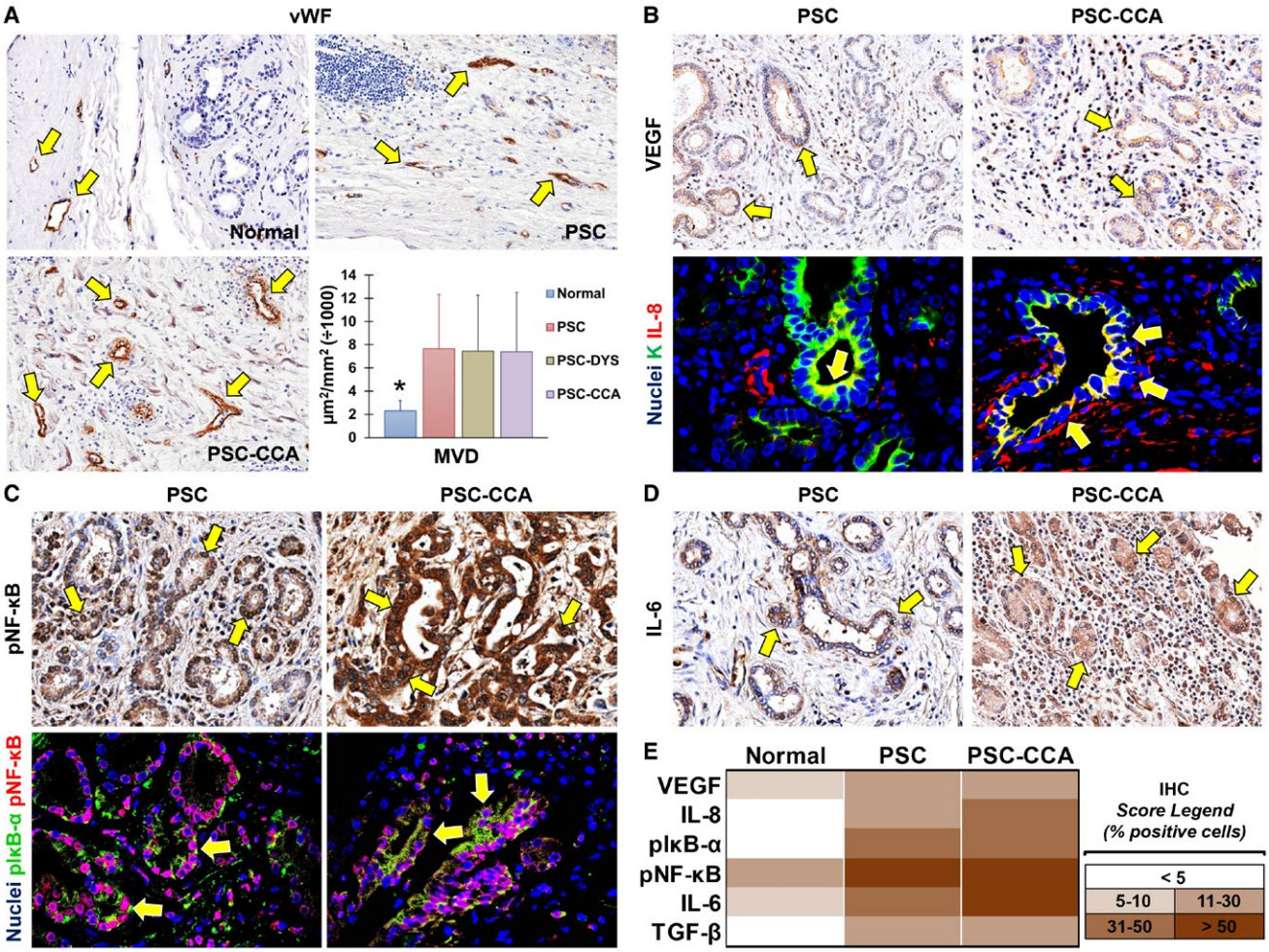

FIG. 3. MVD and inflammatory pathways in PSC-CCA. (A) IHC for vWF in normal ducts, in ducts affected by PSC, and in PSC-CCA ducts affecting PBGs. MVD, calculated as area occupied by vWF$^+$ vessels (arrows), was higher in ducts affected by PSC and by CCA compared to normal ducts, as summarized by the histogram. Original magnification, ×10. $^*P < 0.05$ versus other groups. (B) IHC for VEGF and IF for pan-cytokeratin (K) and IL-8 in PSC and in PSC-CCA. PBGs in PSC ducts and tumor glands in PSC ducts with CCA showed high expression of VEGF (arrows in upper images). Original magnification, ×20. In lower images, tumor glands expressed higher IL-8 levels compared to PBGs in PSC. Original magnification, ×40. Nuclei are displayed in blue. (C) IHC for pNF-κB and IF for pNF-κB and pIκB-α in PSC and PSC-CCA. PBGs in PSC patients and tumor glands in PSC patients with CCA showed high nuclear expression of pNF-κB (arrows). In lower images, PBGs in PSC and tumor glands in CCA-PSC highly coexpressed pNF-κB and pIκB-α in the same cells. Original magnification, ×40. Nuclei are displayed in blue. (D) IHC for IL-6 in PSC and PSC-CCA. PBGs in PSC patients and tumor glands in PSC patients with CCA showed progressively higher IL-6 expression (arrows). Original magnification, ×20. (E) Heat map for visual representation of IHC/IF results obtained for given markers. IHC scores are reported as a color gradient heat map where different colors represent statistically significant differences among groups. Representative images for IHC stains in normal ducts and for TGF-β expression are included in the Supporting Information.

inhibitor of kappa B alpha (pIκB-α), IL-6, and transforming growth factor beta (TGF-β) (Fig. 3C-E and Table 1; Supporting Fig. S8). Proliferating PBGs in PSC-affected ducts and tumor glands in PSC-CCA showed a higher nuclear expression of pNF-κB (51.6 ± 13.3% and 59.2 ± 10.1%, respectively) compared to normal ducts (21.1 ± 6.6%; $P < 0.02$ and <0.001, respectively). Similarly, PBGs in PSC-affected ducts and tumor glands in PSC-CCA showed a higher expression of pIκB-α (37.0 ± 6.1% and 36.8 ± 3.8%, respectively) compared to normal ducts (1.6 ± 1.1%, $P < 0.001$).

Moreover, proliferating PBGs in PSC-affected ducts and tumor glands in PSC-CCA showed higher expression of IL-6 (30.0 ± 14.7% and 56.3 ± 4.8%, respectively) compared to normal ducts (6.0 ± 2.7%, $P < 0.05$; Fig. 3D). IL-6 expression in PSC-CCA was higher compared to PBGs in PSC-affected ducts ($P < 0.05$).

Finally, TGF-β expression was higher in PBGs in PSC-affected ducts and in tumor glands in PSC-CCA (17.8 ± 5.3% and 22.0 ± 7.7%, respectively) compared to normal ducts (1.2 ± 0.4%, $P < 0.05$; Supporting Fig. S10).

EXPRESSION OF EMT TRAITS IN PSC AND PSC-CCA

The phenotype of CCA in PSC patients was further characterized by analyzing the expression of EMT traits. CCA glandular elements expressed higher levels of alpha smooth muscle actin (αSMA) and N-cadherin (25.0 ± 7.3% and 15.6 ± 4.2%, respectively) compared to proliferating and dysplastic PBGs in PSC-affected ducts (9.2 ± 2.4% and 6.2 ± 2.9%, respectively; $P < 0.05$; Fig. 4). In keeping with this, CCA glandular elements also coexpressed vimentin and K7 (Supporting Fig. S11). No or only occasional expression of the above-mentioned mesenchymal markers was present in normal specimens (Fig. 4; Supporting Fig. S11).

PRIMARY CILIUM, AUTOPHAGY, AND SENESCENCE IN PSC AND PSC-CCA

The presence of primary cilium in PBGs was evaluated (Fig. 5; Supporting Fig. S12). In normal and in PSC-affected ducts, the percentage of PBG acini displaying primary cilia was 30%-50% (45.2 ± 8.7% and 44.0 ± 9.4%, respectively); this percentage was significantly reduced in dysplastic PBGs in PSC-affected ducts (7.8 ± 2.6%, $P < 0.05$); moreover, primary cilia almost completely disappeared in neoplastic glands in PSC-CCA samples (0.4 ± 0.5%, $P < 0.001$ versus normal and PSC-affected ducts). Interestingly, both PSC-CCA and PSC samples were characterized by an extremely high expression of glioma-associated oncogene 1 (Gli-1; the effector of the Sonic Hedgehog pathway) by PBG cells (71.6 ± 5.9% and 67.4 ± 9.9%, respectively) compared to controls (6.4 ± 2.9%; $P < 0.001$), with no significant differences between PSC-CCA and PSC (Fig. 5F and Table 1; Supporting Fig. S12). Furthermore, histone deacetylase 6 (HDAC6) expression was increased in PSC-CCA (36.6 ± 7.1%; Fig. 5D) compared to PSC-affected ducts (7.8 ± 1.9%, $P < 0.05$) and normal ducts (5.8 ± 2.6%; Supporting Fig. S8).

In regard to autophagy markers (Fig. 5E and Table 1), neoplastic glands in PSC-CCA were characterized by increased expression of light chain 3 (LC3; 40.0 ± 7.1%) compared to PBGs in PSC-affected ducts (12.5 ± 5.0%, $P < 0.05$) and normal ducts (3.2 ± 1.3%, $P < 0.05$; Supporting Fig. S8); this was paralleled by p62 expression, which was higher in neoplastic cells (42.6 ± 6.0%) compared to PBGs in PSC-affected ducts (22.8 ± 5.7%, $P < 0.05$) and normal ducts (2.8 ± 1.9%, $P < 0.01$; Supporting Fig. S8).

Finally, the senescence marker gamma H2A histone family, member x (γH2A.x) was investigated (Fig. 5F and Table 1); neoplastic glands in PSC-CCA and PBGs in PSC-affected ducts were characterized by increased expression of γH2A.x (24.2 ± 5.8% and 23.2 ± 6.6%, respectively) compared to normal ducts (3.0 ± 1.6%, $P < 0.05$; Supporting Fig. S8).

IN VITRO EXPERIMENTS IN hBTSCs AND PRIMARY CULTURES OF HUMAN MUCINOUS CCAs

hBTSCs were exposed *in vitro* to endogenous (i.e., oxysterols) and exogenous (i.e., LPS) compounds already described as cellular stressors associated with PSC.[7,19] The prolonged (i.e., 10 days) exposure to LPS and cholest-4,6-dien-3-one (oxysterols) induced in hBTSCs a marked proliferative effect as demonstrated by the increase of proliferation index (MTS assay) and the significant reduction of population doubling time compared to controls (i.e., KM alone; $P < 0.001$; Fig. 6A). This proliferative effect was further confirmed by WB for PCNA and IF for Ki67 (Fig. 6B,C). Interestingly, exposure to LPS and oxysterols increased expression of the pluripotency genes (i.e., OCT4A, NANOG, and SALL4) ($P < 0.001$ versus KM; Fig. 6D) and of pIκB-α and pNF-κB ($P < 0.001$ versus KM; Fig. 6E) in hBTSCs. In regard to EMT traits, exposure of hBTSCs to LPS and oxysterols determined the increase of genes associated with EMT (i.e., TWIST and αSMA; Fig. 6F). Furthermore,

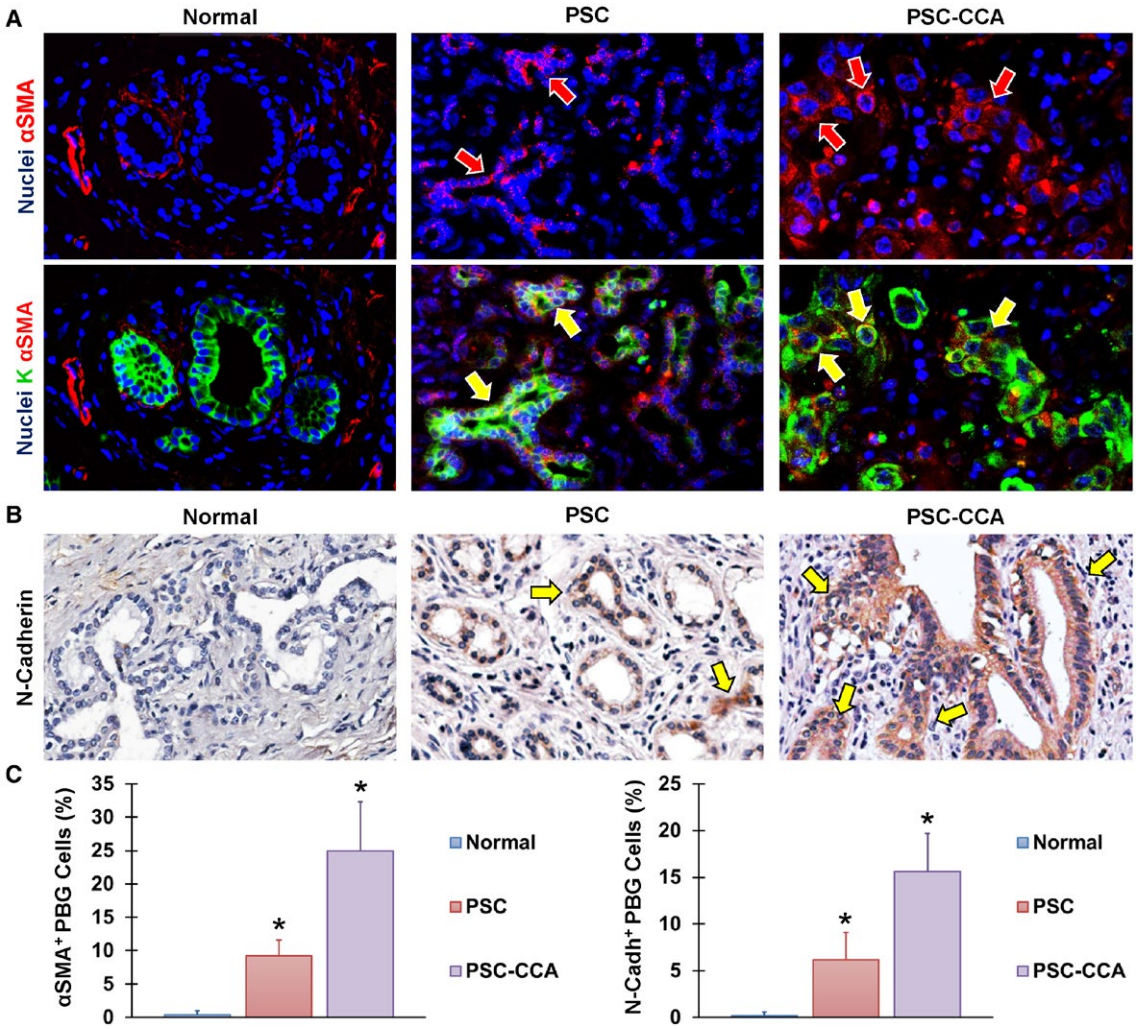

FIG. 4. EMT traits in PSC-CCA. (A) IF for pan-cytokeratin (K) and αSMA in normal ducts, in ducts affected by PSC, and in PSC ducts affected by CCA. In normal ducts, no αSMA expression was revealed in PBGs. PBGs in PSC ducts and tumor glands in PSC-CCA showed progressively higher αSMA expression (arrows). Nuclei are displayed in blue. In upper images, the green channel (K) was removed to better visualize αSMA expression. Original magnification, ×20. (B) IHC for N-cadherin in normal ducts, in PSC, and in PSC-CCA. PBGs in PSC ducts and tumor glands in PSC-CCA showed progressively higher levels of N-cadherin$^+$ cells compared to PBGs in normal and PSC ducts (arrows). Original magnification, ×20. (C) Histograms show differences in αSMA and N-cadherin expression among examined groups. $^*P < 0.05$ compared to other groups.

exposure to LPS and oxysterols increased expression of the senescence marker (γH2A.x) compared to controls (Supporting Fig. S13). Primary cell cultures obtained from human mucinous CCA showed higher positivity for pIκB-α compared to hBTSCs maintained in control medium (KM) and increased pNF-κB and γH2A.x expression compared to hBTSCs in all culture conditions (Fig. 6E; Supporting Fig. S13); furthermore, mucinous CCA cells showed higher expression of EMT genes (i.e., SNAIL1 and TWIST) compared to hBTSCs in KM (Fig. 6F).

To further investigate phenotypical changes in hBTSCs, we studied the eventual loss of apical primary cilium in hBTSCs after prolonged exposure to stressors (Fig. 7). Interestingly, when hBTSCs were exposed to LPS and to oxysterols, they partially lost primary cilia as shown by IF for acetylated α-tubulin compared to the human cholangiocyte cell line H69 and hBTSCs in KM alone (Fig. 7A). Human

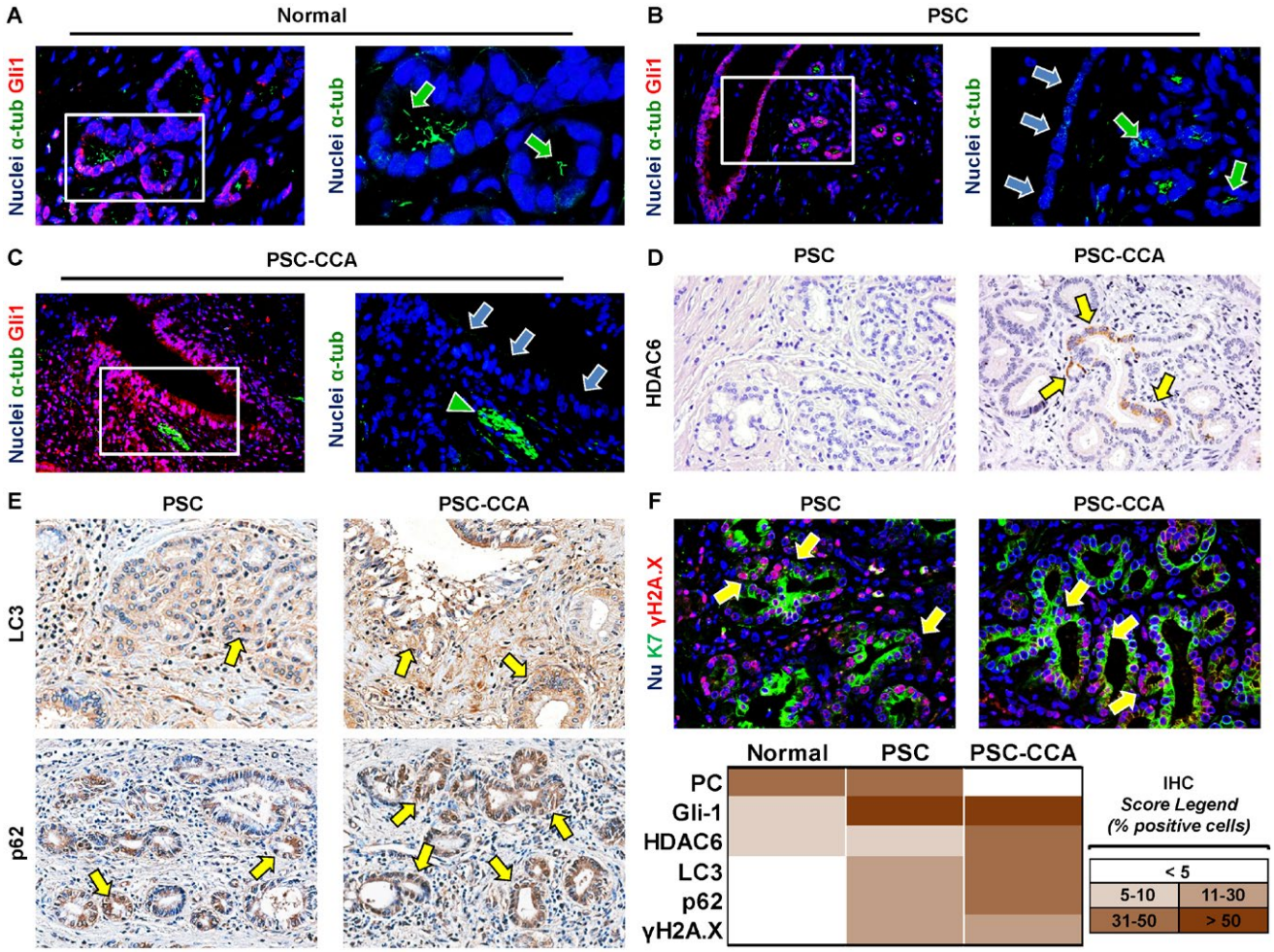

FIG. 5. Primary cilium, autophagy, and senescence markers in PSC-CCA. (A-C) IF for α-acetylated tubulin and Gli-1 in normal ducts (A), in ducts affected by PSC (B), and in PSC ducts affected by CCA. (C) Images on the right represent the magnification of area in the boxes after the removal of the red channel (Gli-1) to better visualize primary cilia. In PSC-CCA, primary cilia in neoplastic cells (blue arrows in C) almost disappeared compared to normal and PSC ducts (green arrows in A and B). PBGs with dysplasia showed no primary cilia (blue arrows in B). Nerves within the section plane are used as positive control (arrowheads) for α-tubulin in (C). Irrespective of the presence of primary cilia, nuclear Gli-1 expression was increased in PSC and PSC-CCA compared to controls (purple cells). Nuclei are displayed in blue. Original magnification, ×40. (D) IHC for HDAC6 in PSC and in PSC-CCA. HDAC6 expression was increased in tumor glands in PSC-CCA (arrows) compared to PBGs in PSC samples. Original magnification, ×40. (E) IHC for LC3 and p62 in PSC and in PSC-CCA. Tumor glandular elements in PSC-CCA were characterized by increased expression of LC3 and p62 (arrows) with respect to PBGs in PSC ducts without CCA. Original magnification, ×40. (F) IF for K7 and the senescence marker γH2A.x in ducts affected by PSC and by PSC-CCA. PBGs in PSC and neoplastic glands in PSC-CCA showed increased expression of γH2A.x, accounting for 11%-30% of their cells. The heat map shows a visual representation of IHC/IF results obtained for given markers. IHC scores are reported as a color gradient heat map where different colors represent statistically significant ($P < 0.05$) differences among groups. Representative images for HDAC6, LC3, p62, and γH2A.x in normal ducts are included in the Supporting Information. Abbreviation: α-tub, α-acetylated tubulin.

mucinous CCA cells were mostly devoid of primary cilia. hBTSCs exposed to LPS and to oxysterols and CCA cells showed higher expression of the *HDAC6* gene and higher punctate LC3 expression compared to the basal condition (i.e., KM; $P < 0.05$; Fig. 7B). Accordingly, hBTSCs exposed to LPS and oxysterols and CCA cells showed higher expression of p62 compared to hBTSCs in KM ($P < 0.05$) as demonstrated by both IF and WB analyses (Fig. 7C). Activation of the autophagy pathway in hBTSCs exposed to LPS

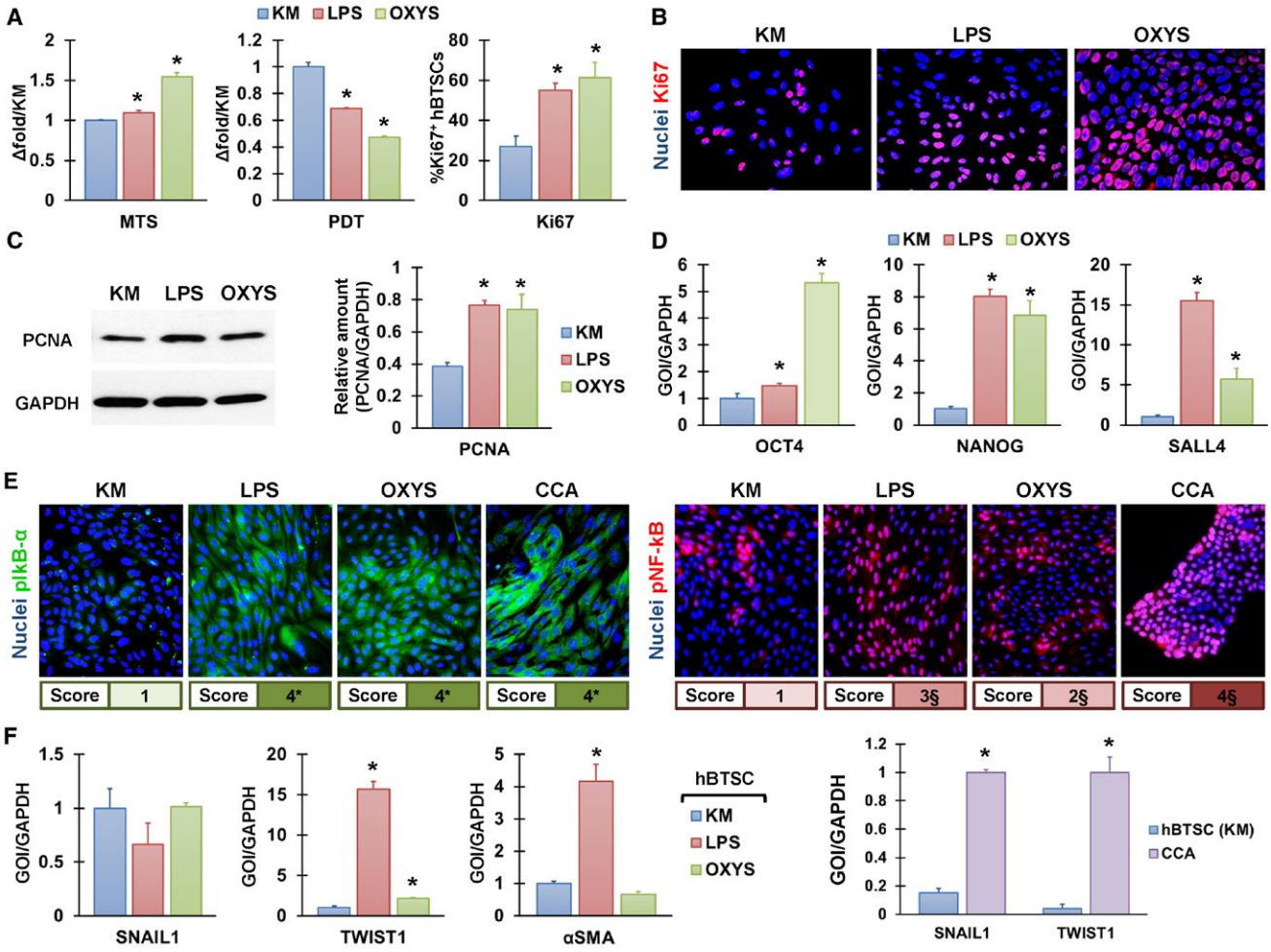

FIG. 6. Effects of LPS and oxysterols in hBTSCs and CCA cells. (A-C) Proliferative effects of prolonged *in vitro* exposure (10 days) to LPS and oxysterols (cholest-4,6-dien-3-one) in hBTSCs. Exposure to LPS and OXYS significantly induced proliferation in hBTSCs as demonstrated by MTS assay and population doubling time (A), by IF for Ki67 (B), and by WB for PCNA (C). $^{*}P < 0.05$ versus controls (KM alone). Nuclei are displayed in blue. Original magnification, ×40. (D) Real-time PCR analysis for OCT4A, NANOG, and SALL4 genes. Exposure to LPS and OXYS induced the expression of pluripotency genes in hBTSCs. $^{*}P < 0.001$ versus KM. (E) *In vitro* expression of pIκB-α and NF-κB by IF in cell cultures. Nuclear pNF-κB and pIκB-α expression was higher in hBTSCs exposed to LPS and OXYS compared to KM. pNF-κB expression was also investigated in primary cell lines obtained from human mucinous CCA. Nuclei are displayed in blue. Original magnification, ×40. Positivity scores for IF are reported in the boxes below the images (0, <5%; 1, 5%-10%; 2, 11%-30%; 3, 31%-50%; 4, >50% positive cells). $^{*}P < 0.05$ versus KM, $^{\S}P < 0.05$ versus all other groups. (F) Real-time PCR for EMT genes in hBTSCs and in CCA cells. Exposure to LPS and OXYS determined increased expression of EMT genes in hBTSCs (i.e., *TWIST1* and α*SMA*) compared to KM. Expression of *SNAIL1* and *TWIST1* was significantly higher in primary human mucinous CCA cells compared to hBTSCs in KM. $^{*}P < 0.05$ versus other groups. Data in the histograms are expressed as means ± standard deviation. Abbreviations: GAPDH, glyceraldehyde 3-phosphate dehydrogenase; GOI, gene of interest; OXYS, cholest-4,6-dien-3-one; PDT, population doubling time.

and oxysterols and in CCA cells was further confirmed by the increase of LC3-II isoform by WB (Fig. 7D). Notably, administration of an autophagy inhibitor (i.e., wortmannin) to cultured cells determined a significant reduction of LC3-II (Fig. 7D) and p62 (Supporting Fig. S14) compared to culture media without wortmannin.

Discussion

The main results in our study indicate that (1) CCAs which arise in patients with PSC are mucinous carcinomas characterized by a high expression of stem/progenitor cell markers and by the primary involvement of PBGs; (2) tumorigenesis in PSC is

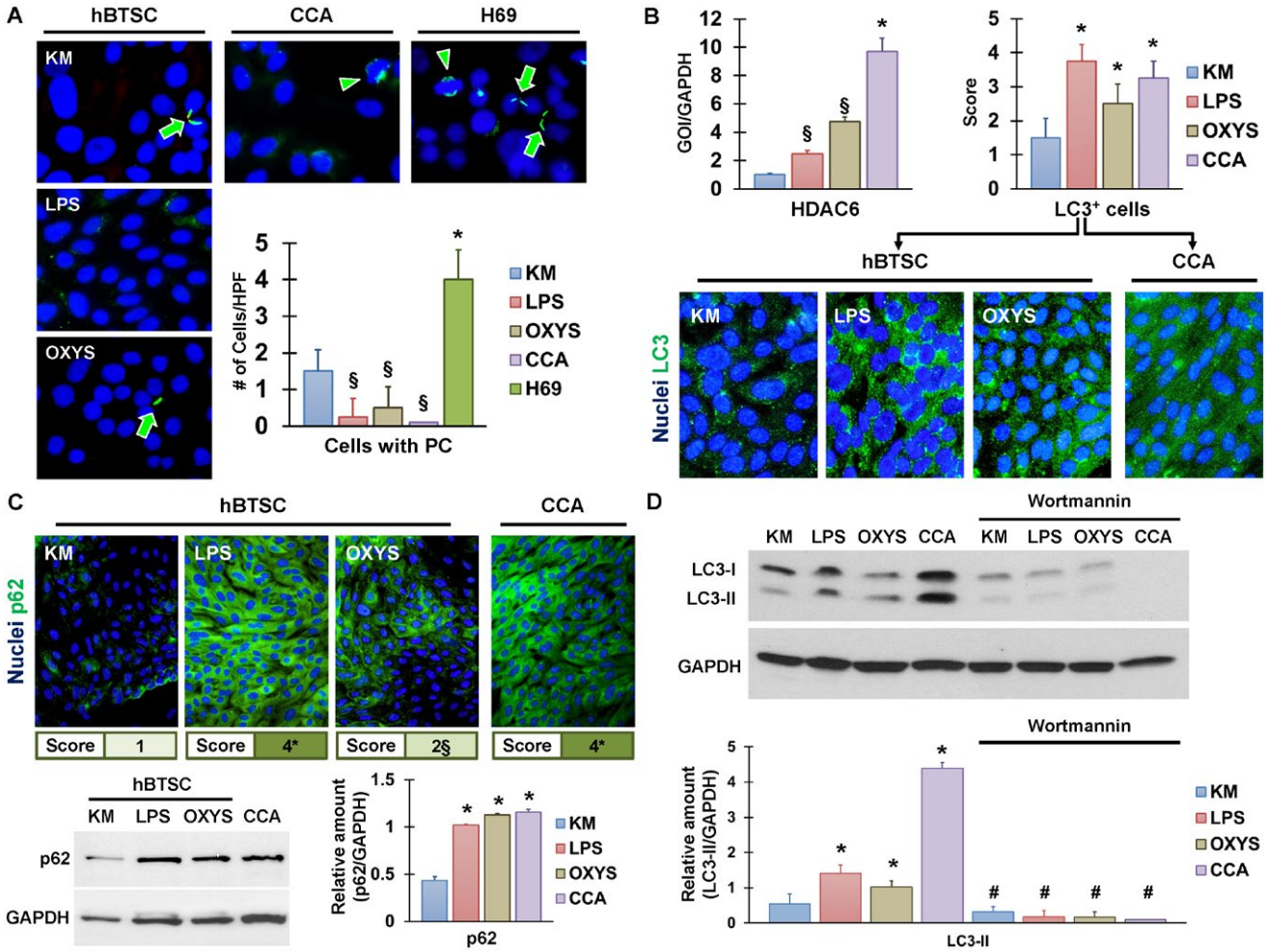

FIG. 7. Primary cilium and autophagy in hBTSCs and CCA cells. (A) *In vitro* expression of α-acetylated tubulin by IF in cell cultures. The presence of primary cilium (arrows) in cell cultures was evaluated. Prolonged *in vitro* exposure (10 days) to LPS and oxysterols (cholest-4,6-dien-3-one) determined in hBTSCs the loss of primary cilia. **P* < 0.01 compared to all other groups, §*P* < 0.05 versus hBTSCs in control conditions (i.e., KM). The human cholangiocyte cell line H69 was used as a positive control as ciliated cells. Mitotic cells display α-acetylated tubulin positivity in the mitotic spindle (arrowheads) and were used as an internal positive control. Nuclei are displayed in blue. Original magnification, ×40. Histogram indicates the number of cells with primary cilia per high-power field. (B) Real-time PCR (left histogram) for the *HDAC6* gene showed that CCA cultures and hBTSCs exposed to LPS and to OXYS have higher expression of *HDAC6* compared to the basal condition (i.e., KM). The right histogram shows the positivity score of punctate LC3 expression in given conditions. Representative stains are placed below the histogram. Nuclei are displayed in blue. Original magnification, ×40. **P* < 0.05 versus other groups, §*P* < 0.05 versus LPS. (C) IF and WB for p62 in cell cultures. hBTSCs exposed to LPS and OXYS and CCA cells showed higher p62 expression and protein amount compared to hBTSCs in basal medium (i.e., KM). Nuclei are displayed in blue. Positivity scores for IF are reported in the boxes below the images (0, <5%; 1, 5%-10%; 2, 11%-30%; 3, 31%-50%; 4, >50% positive cells). Original magnification, ×40. **P* < 0.05 versus KM, §*P* < 0.05 versus other groups. (D) Western blot for LC3-I and LC3-II. Human BTSCs exposed to LPS and OXYS and CCA cells showed higher LC3-II protein amount compared to hBTSCs in KM. **P* < 0.05 versus KM. Administration of wortmannin reduced LC3-II protein amount compared to the same condition without wortmannin. #*P* < 0.05 versus same condition without wortmannin. Data in the histograms are expressed as means ± standard deviation. Abbreviations: GAPDH, glyceraldehyde 3-phosphate dehydrogenase; GOI, gene of interest; HPF, high-power field; OXYS, cholest-4,6-dien-3-one; PC, primary cilia.

a multifocal and multistep process which simultaneously involves several ducts and is preceded by preneoplastic lesions; (3) CCA onset in PSC is associated with chronic inflammation of the bile ducts affected by PSC and with the progressive thickening of duct walls, mostly due to both activation of the BTSC

niche within the PBGs and expansion of the peribiliary vascular plexus; (4) at the cellular level, the pathogenic hyperplasia–dysplasia–carcinoma sequence in PBGs is characterized by the acquisition of EMT features, the absence of primary cilia, and the increase of autophagy and senescence.

CCA development is a major risk factor in PSC and represents the predominant cause of PSC-related death.[7] Depending on the location,[1] PSC-CCA involved hepatic ducts (perihilar CCA), segmental intrahepatic bile ducts (intrahepatic CCA), and bile duct (distal CCA). Examination of the surrounding liver tissues and neighboring extrahepatic biliary tree revealed the presence of synchronous lesions and preneoplastic lesions in the same patient. Histologically, all tumors and synchronous lesions were composed of PAS^+ large ductular structures lined by columnar cells; thus, all examined CCAs can be categorized histologically as large bile duct–type (mucinous) CCAs.

The multifocal synchronous CCA evolution in patients with PSC seems to parallel the colorectal carcinogenesis in inflammatory bowel disease (IBD). IBD is clinically and pathogenetically associated with PSC. Patients with IBD have an increased risk of colorectal synchronous/metachronous malignancies arising from a field of marked chronic inflammation and closely linked to the extent, duration, and severity of inflammation.[24] In keeping with this, the present study demonstrated that biliary malignancies in patients with PSC were associated with the severity of bile duct inflammation, PBG hyperplasia, and duct wall thickening in the same duct. In PSC-affected ducts, chronic inflammation induces BTSC proliferation and subsequent mucinous metaplasia in PBGs[9]; moreover, inflammation determines the emergence of $SOX9^+/CFTR^-$ (cystic fibrosis transmembrane conductance regulator) immature cells instead of normal mature cholangiocytes ($CFTR^+$/secretin $receptor^+$) in surface biliary epithelium.[12] Translating the IBD tumorigenic model in PSC, these observations indicate that the biliary epithelium in PSC may show aspects of "field cancerization". The phenomenon of field cancerization represents the preconditioning of a large area of epithelium to the future development of neoplastic lesions and has been associated with synchronous carcinogenesis in IBD.[24] Chronic inflammation is critical for field cancerization because it induces somatic mutations or epigenomic alterations and favors those cells (clones) best adapted to the inflamed microenvironment based on apoptosis resistance and replicative capability.[24]

In IBD-related colorectal cancer, field cancerization derives from intestinal stem cells within crypts, given their role in epithelial regeneration and their long life span.[24] A putative origin of field cancerization in PSC could be the $Sox9^+$ cell niche within PBGs. In PSC, BTSCs proliferate extensively, show few signs of cellular senescence, and have been proven to be able to escape immune response.[25] A report based on lineage tracing in mice suggested that cells within PBGs could represent the origin of extrahepatic CCA, which supports our data in patients with PSC.[26] In keeping with this, CCAs in patients with PSC diffusely expressed stem cell markers and primarily involved PBGs, which were largely substituted by neoplastic cells. A second mechanism at the basis of the reported aspects could reside in the dedifferentiation of nonstem cells (i.e., mature cholangiocytes).[27] However, this possibility seems less probable considering that mature cholangiocytes in PSC showed features of cellular senescence, apoptosis, and impaired proliferative capabilities.[19,28-30]

Furthermore, our results parallel evidence on the role of the pancreatic duct glands in pancreatic cancer.[31] Pancreatic duct glands represent the anatomical counterpart of PBG within the pancreas[12] and share a unique stem/progenitor cell population with PBGs. Intriguingly, pancreatic duct glands, in response to chronic pancreatitis, can undergo a hedgehog-mediated mucinous metaplasia with features of pancreatic cancer precursor lesions[31] and form the basal crypt segments of intraductal papillary mucinous neoplasms.[32] Thus, a key role for PDGs in early inflammation-mediated events of pancreatic carcinogenesis was identified, and remarkably, biliary neoplasms and preneoplastic lesions parallel pancreatic diseases both pathologically and pathogenetically.[33]

In summary, our study indicates that carcinogenesis in PSC is a multistep and multifocal process characterized by a chronic inflammation–PBG hyperplasia–mucinous dysplasia–carcinoma sequence. PSC could represent a reliable model for the study of biliary tumorigenesis in humans because bile ducts affected by each consecutive step in the carcinogenesis sequence are present in the same patient.

Furthermore, in the present study, we used PSC-CCA to explore the link between inflammation and BTSCs in carcinogenesis, and we confirmed our data

in a parallel *in vitro* study model. Although etiologic factors associated with PSC are largely unknown, biologically relevant endogenous (e.g., oxysterols) and exogenous (e.g., LPS from bacterial translocation) molecules present in the bile have been tested as stressors to mimic cholangiocyte damage in PSC.[19,34] In general, oxysterols were demonstrated to induce cholangiocyte apoptosis, to perpetuate inflammation in cholangiopathies, and to display mutagenic and carcinogenic properties.[19,34] Moreover, LPS plays a role in activation of the NF-κB pathway[35] and can induce senescence and favor the acquisition of a cytokine secretory phenotype in cholangiocytes. Therefore, we directly tested the effects of LPS and oxysterols on hBTSCs *in vitro*. Prolonged exposure to LPS and oxysterols triggered hBTSC proliferation and increased NF-κB pathway activation and senescence. In keeping with this, the high pIκB-α/pNF-κB expression in PBGs observed in tissue slides is associated with increased γH2A.x expression and enhanced production of cytokines (i.e., IL-6, IL-8, and TGF-β), thus suggesting the acquisition of a senescence-associated secretory phenotype[19] and the existence of a proinflammatory loop. Proliferating BTSCs in PSC expressed elevated levels of VEGF and IL-8, which are associated with increased extension of the peribiliary vascular plexus. The presence of an expanded vascular plexus around PBGs in PSC can further support tumor development and growth along the duct wall. Interestingly, in colitis-associated carcinogenesis, chronic inflammation could induce VEGF release by colonic epithelial cells, supporting tumor development in both an autocrine and a paracrine (angiogenesis) manner.[36]

At the cellular level, the present study demonstrated the possible roles of EMT and cilium disarrangement in the progression from PBG hyperplasia to tumor development. In PSC, the increase of EMT-related markers in neoplastic compared to hyperplastic PBGs is paralleled by the progressive loss of membrane EpCAM positivity, thus indicating the acquisition of a mesenchymal phenotype favoring invasion. In keeping with this, low EpCAM expression was found in neoplastic glands distant from the tumor mass (i.e., small portal tract and distant metastasis). The prolonged *in vitro* exposure of hBTSCs to LPS and oxysterols determined the up-regulation of EMT genes, confirming that PSC-associated endogenous and exogenous stressors can contribute to triggering EMT in hBTSCs. Similarly, CCA cells showed a higher expression of EMT-related genes *in vitro* compared to hBTSCs.

Acquisition of the EMT trait phenotype is associated with the parallel absence of primary cilia in hBTSCs and CCA cells, as observed both in tissue slides and *in vitro*. In tissue slides, we demonstrated that primary cilia in PBGs were reduced in PSC samples and almost completely absent in PSC-CCA samples in parallel with an increased expression of HDAC6 and autophagy markers. *In vitro*, prolonged exposure to LPS and oxysterols reduced the number of ciliated hBTSCs, while CCA cells rarely showed primary cilia; the loss/absence of primary cilia is associated with *HDAC6* gene up-regulation and increased autophagy markers (p62 and LC3-II). In polarized epithelial cells, primary cilia are apical organelles and function as a cellular "antenna" by transducing extracellular signals to the cell body.[37] Interestingly, previous reports have suggested that the loss of primary cilia has a major role in CCA pathogenesis and that its disruption in cholangiocytes is mediated by HDAC6 expression and by autophagy (i.e., ciliophagy).[38] Primary cilia are emerging as an important structure in influencing the proliferation and differentiation of stem cells by the modulation of signaling pathways.[37,39] Interestingly, neoplastic PBGs without primary cilia maintained high expression of Gli-1, suggesting a noncanonical activation of the hedgehog pathway.[39,40] Taken together, our data clearly indicate that PSC carcinogenesis is characterized by the loss of epithelial cell polarization and the acquisition of EMT traits in PBGs and associated BTSCs. Chronic inflammation in PSC could determine the loss of primary cilia in BTSCs by stimulating HDAC6 expression and autophagy. In turn, deciliated BTSCs could be more prone to neoplastic transformation, thus representing a candidate cell of origin for CCA in these patients.

In conclusion, our results demonstrated that PBGs are profoundly involved in CCA which arises in patients affected by PSC. In these patients, CCA represents the final step of several progressive modifications involving PBG cells including proliferation, mucinous metaplasia, loss of primary cilia, and acquisition of EMT trait features. Furthermore, the present study identified autophagy and senescence as key processes in the neoplastic transformation of PBGs and in the expression of a secretory phenotype able to further trigger biliary inflammation.

Importantly, tumor appearance was anticipated by typical morphological modifications which resulted in progressive thickening of the bile ducts and could support forthcoming radiological studies. In this light, bile duct wall thickness, PBG hyperplasia, and peribiliary vascular plexus remodeling could be investigated as surrogate markers to individuate PSC patients with higher PBG proliferation and, possibly, an increased risk of developing CCA. Finally, our results indicate the presence of a progressive tumorigenesis sequence in patients with PSC which could represent a human model for biliary carcinogenesis and could possibly identify specific molecular targets using a multi-omics approach.

Acknowledgment: We are grateful to Melissa Kerr for her help in English proofreading.

REFERENCES

1) Banales JM, Cardinale V, Carpino G, Marzioni M, Andersen JB, Invernizzi P, et al. Expert consensus document: cholangiocarcinoma: current knowledge and future perspectives consensus statement from the European Network for the Study of Cholangiocarcinoma (ENS-CCA). Nat Rev Gastroenterol Hepatol 2016;13:261-280.
2) **Cardinale V**, **Renzi A**, Carpino G, Torrice A, Bragazzi MC, Giuliante F, et al. Profiles of cancer stem cell subpopulations in cholangiocarcinomas. Am J Pathol 2015;185:1724-1739.
3) Massani M, Stecca T, Fabris L, Caratozzolo E, Ruffolo C, Furlanetto A, et al. Isolation and characterization of biliary epithelial and stromal cells from resected human cholangiocarcinoma: a novel *in vitro* model to study tumor–stroma interactions. Oncol Rep 2013;30:1143-1148.
4) Raggi C, Invernizzi P, Andersen JB. Impact of microenvironment and stem-like plasticity in cholangiocarcinoma: molecular networks and biological concepts. J Hepatol 2015;62:198-207.
5) Duffy AG, Makarova-Rusher OV, Greten TF. The case for immune-based approaches in biliary tract carcinoma. Hepatology 2016;64:1785-1791.
6) Tyson GL, El-Serag HB. Risk factors for cholangiocarcinoma. Hepatology 2011;54:173-184.
7) Lazaridis KN, LaRusso NF. Primary sclerosing cholangitis. N Engl J Med 2016;375:1161-1170.
8) Hirschfield GM, Karlsen TH, Lindor KD, Adams DH. Primary sclerosing cholangitis. Lancet 2013;382:1587-1599.
9) Carpino G, Cardinale V, Renzi A, Hov JR, Berloco PB, Rossi M, et al. Activation of biliary tree stem cells within peribiliary glands in primary sclerosing cholangitis. J Hepatol 2015;63:1220-1228.
10) **Cardinale V**, **Wang Y**, Gaudio E, Carpino G, Mendel G, Alpini G, et al. The biliary tree: a reservoir of multipotent stem cells. Nat Rev Gastroenterol Hepatol 2012;9:231-240.
11) **Carpino G**, **Cardinale V**, Onori P, Franchitto A, Berloco PB, Rossi M, et al. Biliary tree stem/progenitor cells in glands of extrahepatic and intraheptic bile ducts: an anatomical in situ study yielding evidence of maturational lineages. J Anat 2012;220:186-199.
12) **Lanzoni G**, **Cardinale V**, Carpino G. The hepatic, biliary, and pancreatic network of stem/progenitor cell niches in humans: a new reference frame for disease and regeneration. Hepatology 2016;64:277-286.
13) **Carpino G**, **Nobili V**, Renzi A, De Stefanis C, Stronati L, Franchitto A, et al. Macrophage activation in pediatric nonalcoholic fatty liver disease (NAFLD) correlates with hepatic progenitor cell response via Wnt3a pathway. PLoS One 2016;11:e0157246.
14) Carpino G, Cardinale V, Folseraas T, Overi D, Floreani A, Franchitto A, et al. Hepatic stem/progenitor cell activation differs between primary sclerosing and primary biliary cholangitis. Am J Pathol 2018;188:627-639.
15) **Cardinale V**, **Wang Y**, Carpino G, Cui CB, Gatto M, Rossi M, et al. Multipotent stem/progenitor cells in human biliary tree give rise to hepatocytes, cholangiocytes, and pancreatic islets. Hepatology 2011;54:2159-2172.
16) **Carpino G**, **Cardinale V**, Gentile R, Onori P, Semeraro R, Franchitto A, et al. Evidence for multipotent endodermal stem/progenitor cell populations in human gallbladder. J Hepatol 2014;60:1194-1202.
17) Fraveto A, Cardinale V, Bragazzi MC, Giuliante F, De Rose AM, Grazi GL, et al. Sensitivity of human intrahepatic cholangiocarcinoma subtypes to chemotherapeutics and molecular targeted agents: a study on primary cell cultures. PLoS One 2015;10:e0142124.
18) Masyuk AI, Huang BQ, Radtke BN, Gajdos GB, Splinter PL, Masyuk TV, et al. Ciliary subcellular localization of TGR5 determines the cholangiocyte functional response to bile acid signaling. Am J Physiol Gastrointest Liver Physiol 2013;304:G1013-G1024.
19) **Tabibian JH, O'Hara SP,** Splinter PL, Trussoni CE, LaRusso NF. Cholangiocyte senescence by way of N-ras activation is a characteristic of primary sclerosing cholangitis. Hepatology 2014;59:2263-2275.
20) Sheth P, Delos Santos N, Seth A, LaRusso NF, Rao RK. Lipopolysaccharide disrupts tight junctions in cholangiocyte monolayers by a c-Src-, TLR4-, and LBP-dependent mechanism. Am J Physiol Gastrointest Liver Physiol 2007;293:G308-G318.
21) Seo DW, Choi HS, Lee SP, Kuver R. Oxysterols from human bile induce apoptosis of canine gallbladder epithelial cells in monolayer culture. Am J Physiol Gastrointest Liver Physiol 2004;287:G1247-G1256.
22) Nevi L, Cardinale V, Carpino G, Costantini D, Di Matteo S, Cantafora A, et al. Cryopreservation protocol for human biliary tree stem/progenitors, hepatic and pancreatic precursors. Sci Rep 2017;7:6080.
23) Bright NA, Lindsay MR, Stewart A, Luzio JP. The relationship between lumenal and limiting membranes in swollen late endocytic compartments formed after wortmannin treatment or sucrose accumulation. Traffic 2001;2:631-642.
24) Choi CR, Bakir IA, Hart AL, Graham TA. Clonal evolution of colorectal cancer in IBD. Nat Rev Gastroenterol Hepatol 2017;14:218-229.
25) Riccio M, Carnevale G, Cardinale V, Gibellini L, De Biasi S, Pisciotta A, et al. Fas/Fas ligand apoptosis pathway underlies immunomodulatory properties of human biliary tree stem/progenitor cells. J Hepatol 2014;61:1097-1105.
26) Nakagawa H, Suzuki N, Hirata Y, Hikiba Y, Hayakawa Y, Kinoshita H, et al. Biliary epithelial injury-induced regenerative response by IL-33 promotes cholangiocarcinogenesis from peribiliary glands. Proc Natl Acad Sci USA 2017;114:E3806-E3815.
27) Guest RV, Boulter L, Kendall TJ, Minnis-Lyons SE, Walker R, Wigmore SJ, et al. Cell lineage tracing reveals a biliary origin of intrahepatic cholangiocarcinoma. Cancer Res 2014;74:1005-1010.

28) **McDaniel K**, **Meng F**, Wu N, Sato K, Venter J, Bernuzzi F, et al. Forkhead box A2 regulates biliary heterogeneity and senescence during cholestatic liver injury in mice. Hepatology 2017;65:544-559.
29) **Tabibian JH**, **Trussoni CE**, O'Hara SP, Splinter PL, Heimbach JK, LaRusso NF. Characterization of cultured cholangiocytes isolated from livers of patients with primary sclerosing cholangitis. Lab Invest 2014;94:1126-1133.
30) Nakanuma Y, Sasaki M, Harada K. Autophagy and senescence in fibrosing cholangiopathies. J Hepatol 2015;62:934-945.
31) Strobel O, Rosow DE, Rakhlin EY, Lauwers GY, Trainor AG, Alsina J, et al. Pancreatic duct glands are distinct ductal compartments that react to chronic injury and mediate Shh-induced metaplasia. Gastroenterology 2010;138:1166-1177.
32) Yamaguchi J, Mino-Kenudson M, Liss AS, Chowdhury S, Wang TC, Fernandez-Del Castillo C, et al. Loss of trefoil factor 2 from pancreatic duct glands promotes formation of intraductal papillary mucinous neoplasms in mice. Gastroenterology 2016;151:1232-1244.
33) Nakanuma Y, Harada K, Sasaki M, Sato Y. Proposal of a new disease concept "biliary diseases with pancreatic counterparts". Anatomical and pathological bases. Histol Histopathol 2014;29:1-10.
34) Kuver R. Mechanisms of oxysterol-induced disease: insights from the biliary system. Clin Lipidol 2012;7:537-548.
35) Luedde T, Schwabe RF. NF-kappaB in the liver—linking injury, fibrosis and hepatocellular carcinoma. Nat Rev Gastroenterol Hepatol 2011;8:108-118.
36) **Wang Y**, **Han G**, **Wang K,** Liu G, Wang R, Xiao H, et al. Tumor-derived GM-CSF promotes inflammatory colon carcinogenesis via stimulating epithelial release of VEGF. Cancer Res 2014;74:716-726.
37) Bodle JC, Loboa EG. Concise review: primary cilia: control centers for stem cell lineage specification and potential targets for cell-based therapies. Stem Cells 2016;34:1445-1454.
38) Gradilone SA, Radtke BN, Bogert PS, Huang BQ, Gajdos GB, LaRusso NF. HDAC6 inhibition restores ciliary expression and decreases tumor growth. Cancer Res 2013;73:2259-2270.
39) Grzelak CA, Sigglekow ND, Tirnitz-Parker JE, Hamson EJ, Warren A, Maneck B, et al. Widespread GLI expression but limited canonical hedgehog signaling restricted to the ductular reaction in human chronic liver disease. PLoS One 2017;12:e0171480.
40) Dhanyamraju PK, Holz PS, Finkernagel F, Fendrich V, Lauth M. Histone deacetylase 6 represents a novel drug target in the oncogenic Hedgehog signaling pathway. Mol Cancer Ther 2015;14:727-739.

Author names in bold designate shared co-first authorship.

Supporting Information

Additional Supporting Information may be found at onlinelibrary.wiley.com/doi/10.1002/hep.30210/suppinfo.